

21. Supplementary Web material is available on Science Online at www.sciencemag.org/cgi/content/full/294/5549/2152/DC1.
22. A blind intercomparison study conducted with Lohmann revealed that after normalization for a 2.4- μ g average difference between his weight measurements and ours, the mean difference between his measurements and ours was about 2 μ g. The range of individual shell weights suggests that if 50 shells are weighed, there is a statistical uncertainty of between 1 and 2 μ g resulting from the finite number of shells weighed. Finally, 15 Holocene samples from a core at 2.3-km depth on the Ontong Java Plateau yielded a mean deviation of 1.5 μ g.
23. D. Archer, S. Emerson, C. Reimers, *Geochim. Cosmochim. Acta* **53**, 2831 (1989).
24. S. R. Emerson, D. Archer, *Philos. Trans. R. Soc. London Ser. A* **331**, 29 (1990).
25. B. Hales, S. Emerson, D. Archer, *Deep-Sea Res.* **41**, 695 (1994).
26. B. Hales, S. Emerson, *Global Biogeochem. Cycles* **10**, 527 (1996).
27. W. R. Martin, F. L. Sayles, *Geochim. Cosmochim. Acta* **60**, 243 (1996).
28. B. Hales, S. Emerson, *Geochim. Cosmochim. Acta* **61**, 501 (1997).
29. E. A. Boyle, *Paleoceanography* **3**, 471 (1988).
30. D. W. Lea, E. A. Boyle, *Nature* **347**, 269 (1990).
31. ———, *Paleoceanography* **5**, 719 (1990).
32. T.-H. Peng, W. A. Broecker, *Global Biogeochem. Cycles* **1**, 155 (1987).
33. W. S. Broecker, T.-H. Peng, *Nature* **356**, 587 (1992).
34. W. B. Curry, J. C. Duplessy, L. D. Labeyrie, N. J. Shackleton, *Paleoceanography* **3**, 317 (1988).
35. W. S. Broecker, T.-H. Peng, S. Trumbore, G. Bonani, W. Wolfli, *Global Biogeochem. Cycles* **4**, 103 (1990).
36. W. S. Broecker, E. Clark, *GC000151* (2001).
37. W. S. Broecker, J. Lynch-Stieglitz, E. Clark, I. Hajdas, G. Bonani, *GC000177* (2001).
38. K. Matsumoto et al., *Earth Planet. Sci. Lett.* **192**, 319 (2001).
39. We are indebted to P. Lohmann for steering us away from our size index method and toward his shell weight method. He also helped us get started and worked with us to intercalibrate our measurements with his. Samples for this study were supplied by Woods Hole Oceanographic Institute's W. Curry (Ceara Rise) and D. McCorkle (Ontong Java Plateau). We also acknowledge R. Lotti for access to the Lamont-Doherty Earth Observatory (LDEO) core collection. Support for this research was provided by National Science Foundation grant OCE-00-81809. This is LDEO contribution 6259.

6 July 2001; accepted 15 October 2001

Requirement of *Math1* for Secretory Cell Lineage Commitment in the Mouse Intestine

Qi Yang,¹ Nessim A. Bermingham,^{2,4} Milton J. Finegold,³ Huda Y. Zoghbi^{1,2,4*}

The mouse small intestinal epithelium consists of four principal cell types deriving from one multipotent stem cell: enterocytes, goblet, enteroendocrine, and Paneth cells. Previous studies showed that *Math1*, a basic helix-loop-helix (bHLH) transcription factor, is expressed in the gut. We find that loss of *Math1* leads to depletion of goblet, enteroendocrine, and Paneth cells without affecting enterocytes. Colocalization of *Math1* with Ki-67 in some proliferating cells suggests that secretory cells (goblet, enteroendocrine, and Paneth cells) arise from a common progenitor that expresses *Math1*, whereas absorptive cells (enterocytes) arise from a progenitor that is *Math1*-independent. The continuous rapid renewal of these cells makes the intestinal epithelium a model system for the study of stem cell regeneration and lineage commitment.

The mouse gut begins developing at embryonic day 7.5 (E7.5). Invagination of the most anterior and posterior endoderm leads to the formation of the foregut and hindgut pockets, respectively, which extend toward each other and fuse to form the gut tube. By E15.5, the gut appears as a poorly differentiated, pseudostratified epithelium. From E15.5 to E19, nascent villi with a monolayer of epithelial cells develop in a duodenum-to-colon pattern. During the first two postnatal weeks, the intervillus epithelium, where proliferating and less differentiated cells reside, develops into the crypts of Lieberkühn. Stem cells in the intervillus epithelium (during embryogen-

esis) or crypts (in adulthood) give rise to four principle cell types: absorptive enterocytes or columnar cells, mucous-secreting goblet cells, regulatory peptide-secreting enteroendocrine cells in the large and small intestines, and antimicrobial peptide-secreting Paneth cells in the small intestine only. Enterocytic, goblet, and enteroendocrine cells continue to differentiate and mature while migrating up the villus, and are finally extruded into the lumen at the tip. This journey takes about 2 to 3 days. The Paneth cells migrate downward and reside at the base of the crypt for ~21 days before being cleared by phagocytosis (1–3).

The epithelial-mesenchymal interaction has been shown to be critical in the proximal-distal, crypt-villus patterning during gut development. A number of signaling molecules and transcription factors are involved in these processes (4–7). Previous studies have suggested that all four epithelial cell lineages originate from a common ancestor (1–3, 8), but the mechanisms

that control the epithelial lineage differentiation are not well understood. T cell factor-4 (*Tcf4*) plays a role in the stem cell maintenance in the small intestine but does not induce epithelial cells to differentiate into enterocytes or goblet cells (9). Because *Math1* is expressed in the gut (10) and involved in cell fate determination in the nervous system (11, 12), we sought to determine its function during gut development.

We have two null alleles for *Math1*: *Math1*^{−/−} (with the coding region replaced by *Hprt*) and *Math1*^{β-Gal/β-Gal} (with the coding region replaced by the β-galactosidase gene, which is then expressed under the control of the *Math1* promoter) (11). *Math1* null mice die shortly after birth, but *Math1* heterozygous mice survive to adulthood and appear normal. We previously showed that *Math1*/*LacZ* expression faithfully mimics the endogenous gene expression (11). Here we used *Math1*^{β-Gal/−} instead of *Math1*^{β-Gal/β-Gal} null mice for X-gal staining experiments to ensure equal copy numbers of the *LacZ* gene in heterozygous and null animals.

Math1/*LacZ* expression within the gut is restricted to the intestinal epithelium starting at E16.5 and is sustained until adulthood (13). We detected no *Math1*/*LacZ* expression in the stomach, pancreas, or lung. In E18.5 heterozygous mice, *LacZ*-positive cells are sparsely scattered in the villi, the intervillus epithelium (Fig. 1A), and colonic crypts (Fig. 1C). In *Math1* null littermates, however, *LacZ*-expressing cells are clustered in the intervillus region of ileum (Fig. 1B) and at the bases of the colonic crypts (Fig. 1D). *Math1*/*LacZ* expression persists throughout duodenum, jejunum, ileum, and colon [Fig. 1, E and F, and Web fig. 1 (14)] in adult *Math1*^{β-Gal/+} mice. In the villi, the scattered blue cells appear to have a goblet cell morphology (a spherical vacuole); at the base of the crypt, most apical granule-containing Paneth cells appear to be *LacZ*-positive. X-gal stained cells are also found in the mid-crypt region. *LacZ* expression in adult crypts suggests that *Math1* helps initiate cytodifferentiation of the epithelial cells.

We detected no *Math1*/*LacZ* expression

¹Department of Pediatrics and Program in Developmental Biology, ²Department of Molecular and Human Genetics, ³Department of Pathology and ⁴Howard Hughes Medical Institute, Baylor College of Medicine, Houston, TX 77030, USA.

*To whom correspondence should be addressed. E-mail: hzyoghbi@bcm.tmc.edu

Fig. 1. *Math1/LacZ* expression detected by X-gal staining. *Math1/LacZ* expression in E18.5 intestines (A to D). Cross section of *Math1* ^{β -Gal/+} ileum (A) and colon (C), *Math1* ^{β -Gal/-} ileum (B) and colon (D); Arrows indicate sparse *lacZ*-positive cells in heterozygous animals. *Math1/LacZ* expression in 5-month-old *Math1* ^{β -Gal/+} mice (E and F). Longitudinal section of jejunum (E) and colon (F). Original magnification, $\times 400$.

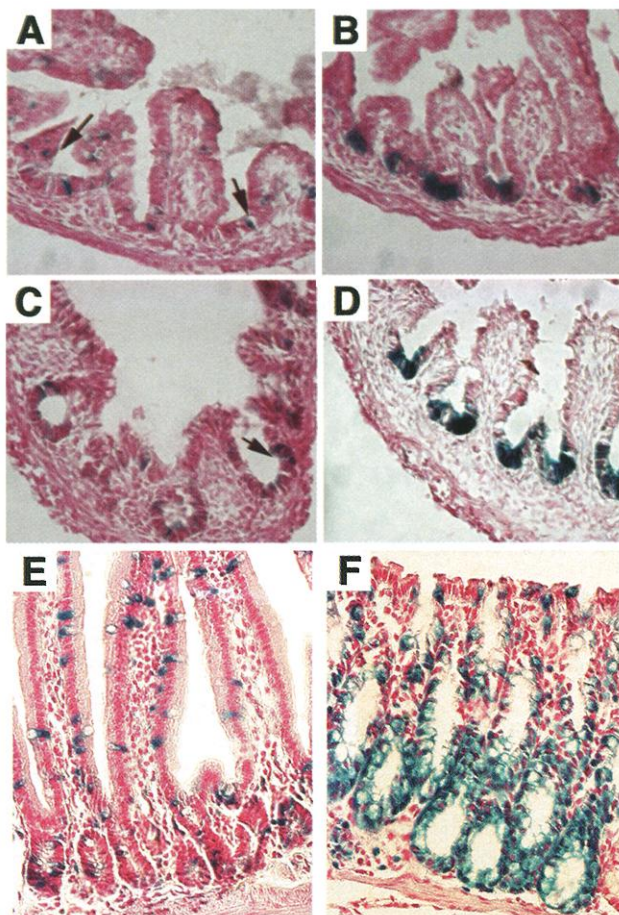
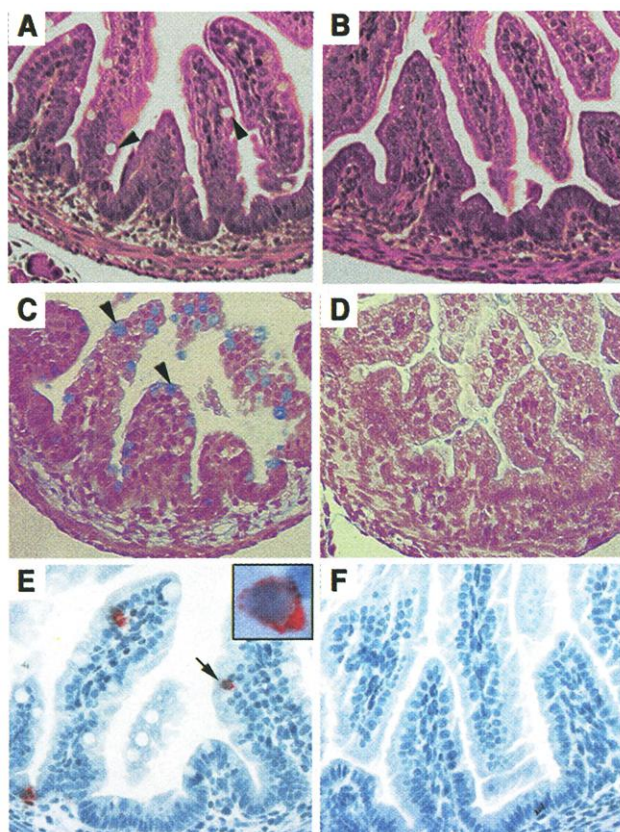


Fig. 2. Lack of goblet and enteroendocrine cells in E18.5 intestines. H&E staining reveals several goblet cells in wild-type duodenum [arrowheads in (A)] and none in null mutant (B); Alcian blue staining shows positively stained goblet cells in wild-type ileum [arrowheads in (C)] but none in *Math1* ^{β -Gal/-} null ileum (D). Serotonin-positive enteroendocrine cells [red-stained cells in (E), the arrow points to the cell enlarged in the inset] are evident in wild-type (E) but not *Math1* ^{β -Gal/-} (F) jejunum. Original magnification, $\times 200$.



in the enteric nervous system (intestinal) from E14.5 to adult. An acetylcholinesterase activity assay (15) revealed no gross abnormalities in the enteric neurons (16), although subtle deficits may not be apparent at these resolutions.

The small and large intestines of *Math1* null embryos (E14.5 to E18.5) showed normal villus architecture, lamina propria, and musculature, but no goblet cells (Fig. 2, A and B). In wild-type animals Alcian blue-positive goblet cells increased in number along the duodenal-colonial axis (Fig. 2C), but were not detected in *Math1* ^{β -Gal/-} mice (Fig. 2D).

We then analyzed the enteroendocrine lineage in the gut epithelium. Neither pan-enteroendocrine markers (chromogranin A, synaptophysin) or specific endocrine markers (glucagon, gastrin, somatostatin, neurotensin, and serotonin) (17) were detectable in any regions of *Math1* ^{β -Gal/-} null mouse intestine (Fig. 2F; cf. wild type, Fig. 2E).

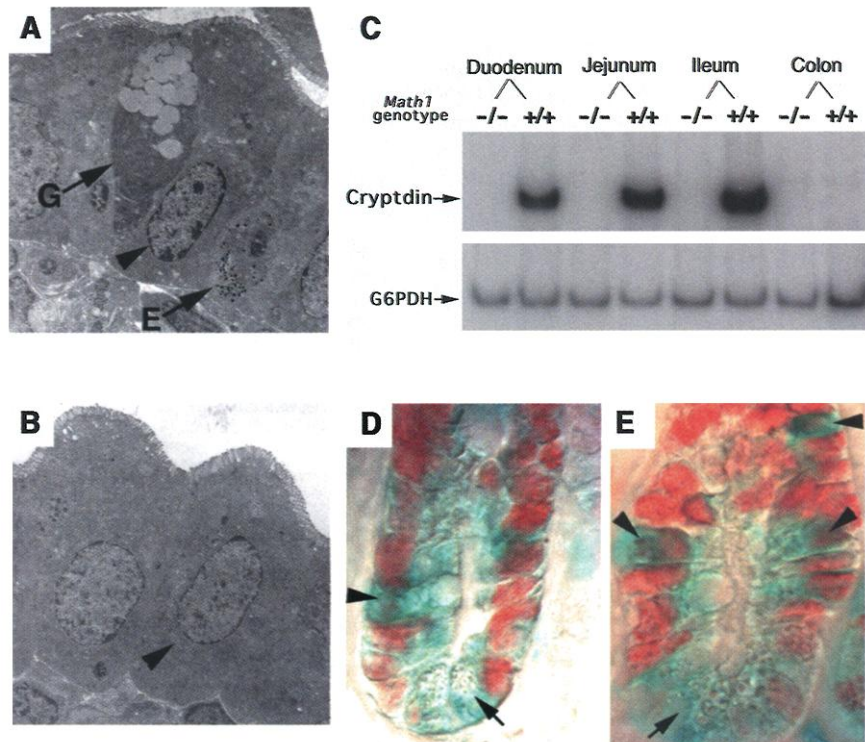
Electron microscopy (EM) on E18.5 embryos (17) revealed no granular or common goblet or enteroendocrine cells in any region of *Math1* ^{β -Gal/-} null mouse intestines (Fig. 3B, cf. wild type in 3A). Null mouse enterocytes, however, had a normal microvillus brush border: strongly positive for alkaline phosphatase and lactase, ample endoplasmic reticulum, a few secondary lysosomes, and regular columnar height with uniform nuclei close to the inner aspect of the cell [Fig. 3B, Web fig. 2 (14)]. Some mutant enterocytes have abundant glycogen (16), like immature enterocytes, whereas wild-type enterocytes no longer have cytoplasmic clusters.

Electron microscopy cannot be used to evaluate Paneth cells in *Math1* null animals, because their characteristic apical granules do not mature until after birth (18). But cryptdin-1 is one of the earliest markers expressed in Paneth cells, starting at E15.5 (19), so we examined its expression (20). Cryptdin-1 consensus primers were used to amplify a 272-bp product corresponding to nucleotides 80 to 352 (21). Cryptdin-1 expression was detected in wild-type duodenum, jejunum, and ileum but was completely absent in these three regions in *Math1* null animals (Fig. 3C). As expected (19), we detected no cryptdin-positive cells in wild-type or *Math1* null colon (Fig. 3C). Neither EM nor tunnel assays revealed signs of premature cell death in *Math1* null gut [Fig. 3B and (16)].

In adult crypts, epithelial stem cells and multipotent progenitor cells are proliferating and show nuclear staining for Ki-67, a cell proliferation marker (9) (Fig. 3, D and E). In the *Math1* ^{β -Gal/+} mice, the *LacZ*-expressing cells show a cytoplasmic blue staining pattern (11). This feature permits colocalization of *Math1*/β-galactosidase and Ki-67. In the crypts, double-positive

REPORTS

Fig. 3. Electron microscopy, cryptdin RT-PCR and colocalization of *Math1/LacZ* and proliferation marker Ki-67. (A) EM of the ileum reveals goblet cells (G) and enteroendocrine cells (E) in wild-type mice; neither of these secretory cells is formed in the *Math1* null mice (B). Enterocytes [arrowheads in (A) and (B)] appear normal in *Math1* null mice (B). Cryptdin mRNA (C) was detected in wild-type duodenum, jejunum, and ileum, but not in colon, whereas the *Math1* null mutant lacked cryptdin RNA in all intestinal tissues examined. G6PDH mRNA level was used as a control. X-gal and Ki-67 antibody staining (blue cytoplasmic and red nuclear, respectively) in sections from adult duodenum (D) and ileum (E) (no hematoxylin counterstaining was applied). Paneth cells with apical granules, located at the bottom of crypts (arrow), show no Ki-67 staining. A subset of Ki-67-positive cells are also *Math1/LacZ*-positive (arrowheads). Original magnification, $\times 2500$ (A and B), $\times 1000$ (D and E).



cells are scattered from the 4th to 13th cell position from the base of the small intestine and are in the 2nd to 4th position in the colon [Fig. 3, D and E, Web fig. 3 (14); (16)]. Clearly not all Ki-67-positive cells express *Math1*, suggesting that *Math1*-negative progenitors give rise to the enterocytes, whereas *Math1*-expressing progenitors become goblet, enteroendocrine, and Paneth cells. Upon deletion of *Math1*, the latter group of cells fail to differentiate, and their progenitors remain in the proliferating stage, thus accounting for the intense X-gal staining seen in the crypts of null embryos (Fig. 1, B and D). To ascertain the effects of *Math1* deletion on the proliferative status of the secretory lineage progenitors, we examined 2500 Ki-67-positive cells in three pairs of E18.5 *Math1* null and heterozygous mice for *LacZ*-positive staining. We scored double-positive cells as a fraction of the total cycling Ki-67-positive population in E18.5 *Math1* heterozygous and null mouse intestines. The ratio of double-positive to Ki-67-positive cells in *Math1* null animals, from duodenum to colon, was roughly three times that seen in heterozygotes (25 to 68% versus 7 to 22%), supporting the hypothesis that cells lacking *Math1* fail to exit the cell cycle and differentiate.

Previous studies have shown that members of the Notch signaling pathway (e.g., *Mash1*, *Neurogenin 3*, and *NeuroD*) are involved in endocrine cell differentiation (22–24). Deletion of *Hes1*, a Notch signaling component that represses bHLH transcriptional activators, leads to an increased num-

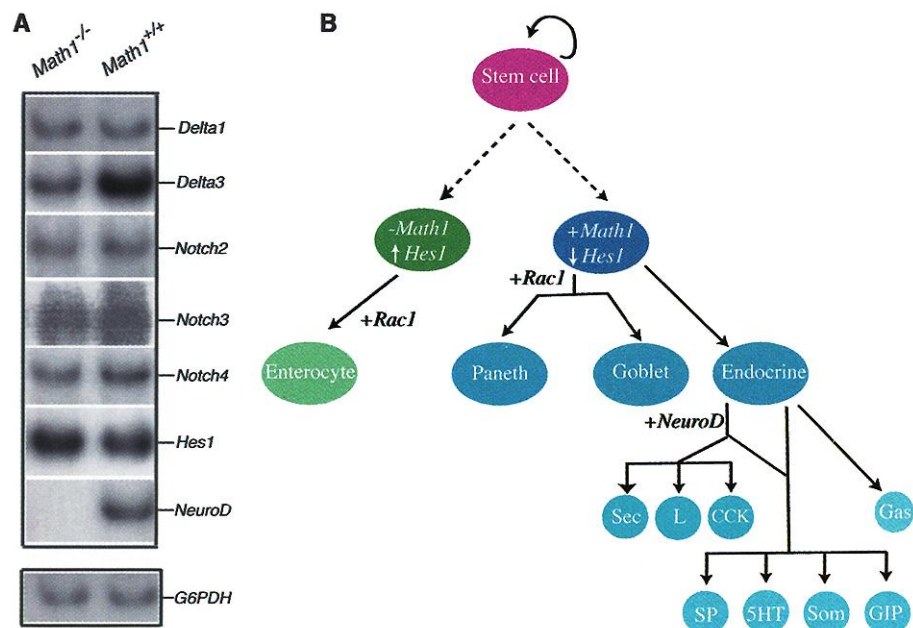


Fig. 4. Expression of Notch components and model for epithelial cell lineage differentiation in mouse intestine. (A) E18.5 small intestines were subjected to RT-PCR using primers specific to the indicated genes. G6PDH mRNA level served as a control. (B) *Math1* is essential for secretory cells. Whether *Math1*-expressing cells descend directly from stem cells or an intermediate progenitor remains unknown. Abbreviations: Sec, secretin; L, glucagon/peptide YY; CCK, cholecystokinin; SP, substance P; 5HT, serotonin; Som, somatostatin; GIP, gastric inhibitory peptide; Gas, gastrin.

ber of enteroendocrine and goblet cells but fewer enterocytes, and elevates expression of *Delta1*, *Delta3*, *NeuroD*, and *Math1* in the small intestine (25). *Hes1* also negatively regulates inner ear hair cell differentiation by suppressing *Math1* (26). These studies support the hypothesis that *Math1* controls cell

fate determination via a Delta-Notch signaling pathway.

Quantitative reverse transcription-polymerase chain reaction (RT-PCR) analysis revealed that *Delta3* was reduced to half of wild-type levels in *Math1* null mice, and *NeuroD* expression was lost completely

(Fig. 4A). In contrast, *Delta1*, *Hes-1*, and *Notch1*, 2, 3, and 4 expression levels and cellular localization of *Hes-1* appeared unaffected [Fig. 4A and Web fig. 4 (14)]. These observations are consistent with previous findings that *Math1* is upstream of *NeuroD* (27) and the notion that *Math1* has a positive feedback effect on Notch ligand (e.g., *Delta3*) expression.

Our findings provide new insight into the role of Notch-mediated lateral inhibition in controlling differentiation of intestinal epithelial lineages. Building on the model set forth by Bjerknes and Cheng (8), we propose that a single self-maintaining stem cell gives rise to two daughter cells directly or through intermediate progenitors (Fig. 4B). In one daughter cell, interaction between Delta and Notch homologs elevates *Hes1* expression, inhibiting *Math1* expression, and this cell adopts an enterocyte fate. In the other daughter cell, lack of *Hes1* expression increases *Math1* expression, and this cell becomes a committed multipotent progenitor that will differentiate into a secretory lineage cell (Fig. 4B). Further differentiation of the secretory lineage into goblet, enteroendocrine, and Paneth cells requires other factors. *NeuroD* has been shown to play a role in differentiation of the secretin and cholecystokinin enteroendocrine cells (24); early committed multipotent endocrine cells can branch into at least three lineages (Fig. 4B) (24). *Rac1* is reported to play a positive role in goblet and Paneth cell differentiation but does not seem to have any impact on the enteroendocrine lineage (18), suggesting that goblet and Paneth cells share a closer relationship during later development. Constitutively activated *Rac1* causes precocious enterocyte growth, indicating its positive role in the absorptive cell lineage (18). These observations suggest that there is cross talk between the Notch and Rho GTPase pathways during formation of the gut epithelium. We cannot yet rule out other models for controlling the secretory and absorptive lineages: e.g., instead of arising from one *Math1*-positive progenitor, the goblet, enteroendocrine, and Paneth cells may differentiate from three distinct progenitors that each express *Math1*. Further study of *Math1* in the mouse intestine will yield deeper insight into the mechanisms controlling production of the different cell types, which may in turn provide therapeutic tools for endocrine and colorectal cancers and regeneration of the intestinal epithelium after injury.

References and Notes

1. H. Cheng, C. P. Leblond, *Am. J. Anat.* **141**, 537 (1974).
2. J. I. Gordon, G. H. Schmidt, K. A. Roth, *FASEB J.* **6**, 3039 (1992).
3. S. P. Bach, A. G. Renehan, C. S. Potten, *Carcinogenesis* **21**, 469 (2000).
4. K. H. Kaestner, D. G. Silberg, P. G. Traber, G. Schutz, *Genes Dev.* **11**, 1583 (1997).

5. O. Pabst, R. Zweigerdt, H. H. Arnold, *Development* **126**, 2215 (1999).
6. F. Beck, F. Tata, K. Chawengsaksophak, *Bioessays* **22**, 431 (2000).
7. J. P. Clatworthy, V. Subramanian, *Mech. Dev.* **101**, 3 (2001).
8. M. Bjerknes, H. Cheng, *Gastroenterology* **116**, 7 (1999).
9. V. Korinek et al., *Nature Genet.* **19**, 379 (1998).
10. C. Akazawa, M. Ishibashi, C. Shimizu, S. Nakanishi, R. Kageyama, *J. Biol. Chem.* **270**, 8730 (1995).
11. N. Ben-Arie et al., *Development* **127**, 1039 (2000).
12. N. A. Bermingham et al., *Neuron* **30**, 411 (2001).
13. X-gal staining of adult intestines was performed as described (18); for embryos, 10- μ M sections from frozen blocks of 4% paraformaldehyde-fixed intestinal tissue were stained overnight at 37°C in a pH 8.0 solution containing 1.3 mM MgCl₂, 15 mM NaCl, 44 mM Hepes buffer (pH 7.3), 3 mM potassium ferri-cyanide, 3 mM potassium ferrocyanide and 0.05% X-gal. Sections were counterstained with nuclear fast red.
14. Supplementary material is available on Science Online at www.sciencemag.org/cgi/content/full/294/5549/2153/DC1
15. E. Blaugrund et al., *Development* **122**, 309 (1996).
16. Q. Yang, H.Y. Zoghbi, unpublished data.
17. Hematoxylin and eosin or Alcian blue and neutral red staining and immunohistochemistry were performed according to standard protocols. The source and final dilution of the primary antibodies were as follows: rabbit chromogranin A antibody (1:2000), gastrin antibody (1:300), glucagon antibody (1:2000), serotonin antibody (1:20000), somatostatin antibody (1:4000), neurotensin antibody (1:2500) are from DiaSorin; rabbit synaptophysin antibody (1:200, BioGenex), and rabbit Ki-67 antibody (1:1000, Novocastra). For EM, different regions of E18.5 intestines were fixed in 3% phosphate-buffered glutaraldehyde and post fixed in phosphate-buffered osmium tetroxide. Specimens were dehydrated and embedded in

Araldite 502 resin. Semithin sections (0.4 μ M) were stained with methylene blue and basic fuchsin. Thin sections (60 nM) were stained with uranyl acetate and lead citrate. The samples were observed on a JEOL 1210 electron microscope.

18. T. S. Stappenbeck, J. I. Gordon, *Development* **127**, 2629 (2000).
19. L. Bry et al., *Proc. Natl. Acad. Sci. U.S.A.* **91**, 10335 (1994).
20. RNA was extracted from E18.5 intestine using TRIzol (Gibco BRL) according to manufacturer's instructions. cDNA synthesis was performed as described (28). Cryptdin and glucose-6-phosphate dehydrogenase (G6PDH) primers and PCR were as previously described (21, 25), except for the thermal cycle profile: a single denaturing step at 96°C for 1 min followed by 25 cycles of 96°C for 30 s; 55°C for 30 s; 73°C for 1 min.
21. D. Darmoul, D. Brown, M. E. Selsted, A. J. Ouellette, *Am. J. Physiol.* **272**, G197 (1997).
22. T. Ito et al., *Development* **127**, 3913 (2000).
23. A. Apelqvist et al., *Nature* **400**, 877 (1999).
24. G. Rindi et al., *Development* **126**, 4149 (1999).
25. J. Jensen et al., *Nature Genet.* **24**, 36 (2000).
26. J. L. Zheng, J. Shou, F. Guillemot, R. Kageyama, W. Gao, *Development* **127**, 4551 (2000).
27. T. Miyata, T. Maeda, J. E. Lee, *Genes Dev.* **13**, 1647 (1999).
28. J. Jensen, P. Serup, C. Karlsen, T. F. Nielsen, O. D. Madsen, *J. Biol. Chem.* **271**, 18749 (1996).
29. We thank S. Henning, K. Zaret, and V. Wang for thoughtful discussions; H. Bellen, B. Hassan, and M.-J. Tsai for critical reading; V. Brandt for thoughtful suggestions on the paper; T. Sudo for *Hes-1* antisense; A. Major, J. Barrish, B. Antalffy, P. Grennan, and M. Fernandez for technical assistance; and M. Gershon for advice on the acetylcholinesterase activity assay. H.Y.Z. is an investigator of the Howard Hughes Medical Institute. Q.Y. is supported by a NASA grant.

24 August 2001; accepted 2 October 2001

Structural Mechanisms of QacR Induction and Multidrug Recognition

Maria A. Schumacher,¹ Marshall C. Miller,¹ Steve Grkovic,² Melissa H. Brown,² Ronald A. Skurray,² Richard G. Brennan^{1*}

The *Staphylococcus aureus* multidrug binding protein QacR represses transcription of the *qacA* multidrug transporter gene and is induced by structurally diverse cationic lipophilic drugs. Here, we report the crystal structures of six QacR-drug complexes. Compared to the DNA bound structure, drug binding elicits a coil-to-helix transition that causes induction and creates an expansive multidrug-binding pocket, containing four glutamates and multiple aromatic and polar residues. These structures indicate the presence of separate but linked drug-binding sites within a single protein. This multisite drug-binding mechanism is consonant with studies on multidrug resistance transporters.

The emergence of multidrug resistance (MDR) has been attributed in part to membrane transport systems capable of effluxing a broad spectrum of toxic compounds (1–4).

In cancer cells, resistance to chemotherapeutic agents is mediated by the P-glycoprotein efflux pump (5, 6), whereas in bacteria MDR transporters are responsible for resistance to many clinically important antimicrobial compounds (7, 8). The serious health threat posed by the emergence of strains of antibiotic-resistant *Staphylococcus aureus* appears to have been exacerbated by plasmid-encoded MDR efflux pumps such as QacA, which confer resistance to monovalent and bivalent

¹Department of Biochemistry and Molecular Biology, Oregon Health & Science University, Portland, OR 97201, USA. ²School of Biological Sciences, A12, University of Sydney, Sydney NSW 2006, Australia.

*To whom correspondence should be addressed. E-mail: brennanr@ohsu.edu